

Proceeding Paper

# Aluminum Beams with Composite Thermal Barriers: Recent Developments in Analysis (Part 1) <sup>†</sup>

James LaBelle

SB Engineering, LLC, Wauwatosa, WI 53222, USA; jlabelle.sbengr@gmail.com

<sup>†</sup> Presented at the 15th International Aluminium Conference, Québec, QC, Canada, 11–13 October 2023.

**Abstract:** Two recent developments in the analysis of aluminum-thermal barrier beams are presented in Part 1 of this paper. These beams are used in windows and curtainwalls to support glass lites. The thermal barriers are more flexible than the aluminum faces, and analysis methods that account for shear deformation are required. Part 1 includes: (1) *New load case*. For a simply supported beam, a closed-form solution for the case of two equal and symmetric concentrated loads has been developed. (2) *Overhang effect*. For a simply supported beam with a midspan concentrated load, an FEA study was conducted regarding the stiffening effect of overhangs for two profiles and shear moduli.

**Keywords:** aluminum; thermal barrier; sandwich beam; curtainwall; shear deformation

## 1. Introduction

Thermal-barrier beams (mullions) are used in windows and curtainwalls to resist wind loads and to reduce both energy loss and condensation. One linear analysis method [1,2] for these beams is an extension of a method [3] developed for sandwich panels. These composite beams consist of extruded aluminum sections joined by a structural insulating material. The connection between the thermal barrier (core) and the facing sections (faces) resists longitudinal shear, thus enabling the composite behavior of these sandwich beams. The core is much less stiff than the aluminum faces; thus, core shear deformation makes these beams more flexible. To address this behavior and aid the design process, the concept of an effective moment of inertia (second area moment,  $I_e$ ), which is less than the full moment of inertia ( $I$ ), has been in use since at least the 1980s. This enables the use of ordinary deflection equations.

Currently, there are two commonly used structural thermal barriers: polyurethane (poured-and-debridged) and glass-fiber reinforced polyamide (nylon) strips. The first type is poured into a cavity connecting two portions of the aluminum extrusion. The aluminum bridge is removed after polyurethane curing. The cavity includes interlocks, as well as staking or indenting at intervals, to better resist wind suction and longitudinal shear. The second type is installed, as a pair of specially shaped strips, into receptor grooves in the facing sections. The exterior sides (“hammers”) of the aluminum grooves are then deformed to achieve firm mechanical contact along the length of the strips. The sides’ contact surfaces have “teeth” (due to knurling) to resist longitudinal shear.

Prior research resulted in the development of closed-form equations to predict the linear response (deflection, stresses and longitudinal shear flow) of this type of composite sandwich beam (simply supported) to four types of symmetrical loading [2] (pp. 43–61): midspan concentrated, uniform, triangular and trapezoidal. These four types represent common cases for fenestration products subject to test loading and wind loading. Other more general loading situations (including response to unsymmetrical loading and a thermal gradient), as well as continuous beams and beams with overhangs, could be analyzed with certain types of finite-element (FEA) software. Thermal-barrier framing has been used in an increasing variety of applications. Thus, to facilitate design, gain deeper



**Citation:** LaBelle, J. Aluminum Beams with Composite Thermal Barriers: Recent Developments in Analysis (Part 1). *Eng. Proc.* **2023**, *43*, 33. <https://doi.org/10.3390/engproc2023043033>

Academic Editor: Mario Fafard

Published: 20 September 2023



**Copyright:** © 2023 by the author. Licensee MDPI, Basel, Switzerland. This article is an open access article distributed under the terms and conditions of the Creative Commons Attribution (CC BY) license (<https://creativecommons.org/licenses/by/4.0/>).

insight into structural behavior and lessen dependence on testing, there is a need to develop additional structural analysis tools.

The developments presented in Part 1 of this article include closed-form linear equations for two symmetric concentrated loads (a simply supported beam without overhangs) and an analytical study of the overhang stiffening of a beam with a midspan concentrated load.

## 2. Two Symmetric Concentrated Loads

In 2014, a doctoral dissertation [4] was published that included the testing, as well as FEA, of thermal-barrier profiles with several different spans, each simply supported and with short overhangs (see Part 2 of the present paper for further study related to that work). The loading consisted of two symmetrically located and equal concentrated loads. This loading was stated to be of interest because of the uniform moment and absence of overall shear in the central region between the loads. This Australian research used a loading arrangement that contrasted with the midspan concentrated loading commonly used in the U.S. testing of thermal-barrier profiles.

Although a beam with two symmetric concentrated loads could be linearly analyzed relatively readily with special FEA software, it was desirable to develop equations (see below) for a closed-form solution, although without overhangs (Figure 1). The necessary mathematical framework for a symmetrical loading that results in differing response regions (a central region and two end regions) had been developed [5] for trapezoidal load as part of a major update of the AAMA TIR-A8 [2].

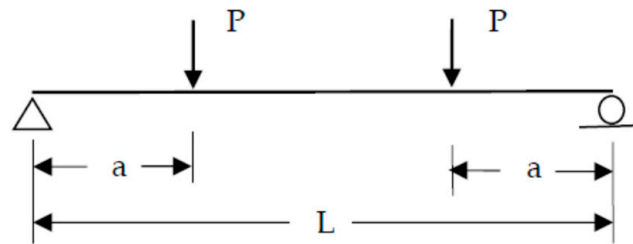


**Figure 1.** Beam with two symmetric loads.

### 2.1. Summary of Governing Equations

The general form of the equations conforms to that used in [2] (pp. 43–61). Background on the development of sandwich beam theory, as applied to an aluminum extrusions composite with structural thermal barriers, is given in [1,2]. The governing fourth-order differential equation relates the deflection to bending moment and shear. The general (complete) solution, consisting of a particular solution plus a complementary (homogeneous) solution, depends on various parameters (beam cross-section properties, span, load type, etc.) and boundary conditions.

For symmetric loading and the central region ( $a \leq x \leq L - a$ ), the general solution to the governing fourth-order differential equation for deflection is:

$$y = D_4x^4 + D_3x^3 + D_2x^2 + D_1x + D_0 + F_1e^p + \frac{F_2}{e^p} \quad (1)$$

For the end region ( $0 \leq x \leq a$ ), the solution is:

$$y = E_4x^4 + E_3x^3 + E_2x^2 + E_1x + E_0 + G_1e^p + \frac{G_2}{e^p} \quad (2)$$

where  $p = x\sqrt{c}$ . The expressions for the integration constants are shown in Tables 1 and 2.

**Table 1.** Constants  $D_0$  to  $D_4$  and  $E_0$  to  $E_4$ .

Constant	$(a \leq x \leq L - a)$	Constant	$(0 \leq x \leq a)$
$D_0$	$\frac{Pa^3}{6EI} - \frac{Pa}{G_p} + \frac{Pa}{cEI}$	$E_0$	0
$D_1$	$-\frac{PaL}{2EI}$	$E_1$	$\frac{-P}{G_p} - \frac{PaL}{2EI} + \frac{Pa^2}{2EI} + \frac{P}{cEI}$
$D_2$	$\frac{Pa}{2EI}$	$E_2$	0
$D_3$	0	$E_3$	$\frac{P}{6EI}$
$D_4$	0	$E_4$	0

**Table 2.** Complementary constants  $F_1, F_2, G_1$  and  $G_2$ .

Load Type	Complementary Constants * **	
Two equal concentrated loads, symmetrical $(a \leq x \leq L - a)$	$F_1$ $\frac{PI_c(e^q - e^{-q})e^{-r}}{2G_p I \sqrt{c}(e^r + e^{-r})}$	$F_2$ $F_1 e^{2r}$
Two equal concentrated loads, symmetrical $(0 \leq x \leq a)$	$G_1$ $F_1 \left( \frac{e^{2q} + e^{2r}}{e^{2q} - 1} \right)$	$G_2$ $-G_1$

\*  $r = 0.5L\sqrt{c}$ . \*\*  $q = a\sqrt{c}$ .

The stress in the facing sections (see Figure 2) is the sum of the axial stress plus that due to bending of that face. The total stress in Face 1, at a distance  $c_{11}$  from the face's centroidal axis, is given by:

$$f_{11} = \frac{-(M - EI_0 y'')}{a_1 D} - Ec_{11} y'' \tag{3}$$

In Face 2, at a distance  $c_{22}$  from the face's centroidal axis, the stress is given by:

$$f_{22} = \frac{M - EI_0 y''}{a_2 D} + Ec_{22} y'' \tag{4}$$

In the above stress equations,  $y'' (=d^2y/dx^2)$  is given by:

$$y'' = 12D_4 x^2 + 6D_3 x + 2D_2 + c \left( F_1 e^p + \frac{F_2}{e^p} \right) \tag{5}$$

For the end regions, we use constants  $E_4, E_3, E_2, G_1$  and  $G_2$  in Equation (5). The approximate shear in the core is found with the following equation:

$$V_c = V - EI_0 y''' \tag{6}$$

Here,  $y''' (=d^3y/dx^3)$  is given by:

$$y''' = 24D_4 x + 6D_3 + c^{1.5} \left( F_1 e^p - \frac{F_2}{e^p} \right) \tag{7}$$

For the end regions, we use constants  $E_4, E_3, G_1$  and  $G_2$  in Equation (7). The shear flow ( $q_c$ ) equals  $V_c/D$ .

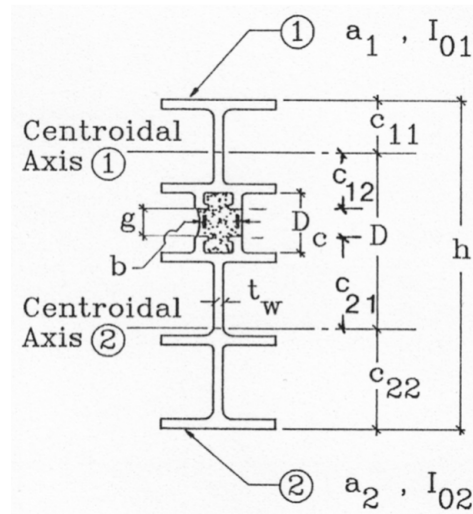


Figure 2. Example profile with geometric notation.

2.2. New Loading Type (Two Equal Concentrated Loads, Symmetrical)

For the particular solution, Table 1 lists the integration constants ( $D_0$  to  $D_4$  and  $E_0$  to  $E_4$ ) for beam analysis for two equal concentrated loads that are symmetrically placed on a simply supported beam. Each load  $P$  is at a distance  $a$  from the near support, where  $0 < a < 0.5L$ . The first set of constants ( $D_0$  to  $D_4$ ) is for the central portion of the span ( $a \leq x \leq L - a$ ), between the two concentrated loads. The second set of constants ( $E_0$  to  $E_4$ ) is for the left end region ( $0 \leq x \leq a$ ), which is the mirror image of the right end region.

Table 2 presents the expressions for the complementary constants.  $F_1$  and  $F_2$  relate to the central portion of the span, and  $G_1$  and  $G_2$  relate to the end region.

The deflection ( $y$ ) at the midspan is used to determine the effective moment of inertia ( $I_e$ ). The second term in Equation (8) is set to zero, and  $d$  is set equal to  $y$  at midspan. Next, both terms in Equation (8) are used to find a more accurate value of the maximum deflection ( $d$ ). Here, the first term (with  $B$ ) accounts for bending and the second term (with  $S$ ) accounts for the shear deformation of the “webs” in the facing sections.  $P^*$  equals the total load ( $2P$ ). The aluminum shear modulus is  $G = 0.375 E$ , the form factor  $F$  can be taken as 1.0 (approximately correct for I-beams), and  $A$  is the area of the facing sections’ webs.

$$d = \frac{P^*L^3}{B} \left( \frac{1}{EI_e} \right) + \frac{P^*L}{S} \left( \frac{F}{AG} \right). \tag{8}$$

Table 3 lists the expressions for  $B$ ,  $S$  and  $P^*$  for bending, as well as a correction for the shear deformation of the aluminum faces.

Table 3. Parameters  $B$ ,  $S$  and  $P^*$ .

Load Type	$B$	$S$	$P^*$
Two equal concentrated loads, symmetrical; ( $k = a/L$ )	$\frac{48}{3k-4k^3}$	$\frac{2}{k}$	$2P$

Another equation for the midspan deflection can be written with the use of the variable  $I'_e$  which includes the effects of shear deformation of the faces:

$$d = \frac{P^*L^3}{BEI'_e}. \tag{9}$$

The expression for  $I'_e$  for this load type (two equal concentrated loads, symmetrical), as a function of  $I_e$ ,  $L$ ,  $k$  and  $A$  is:

$$I'_e = \frac{I_e}{\left[1 + \frac{64I_e}{(3-4k^2)L^2A}\right]} \tag{10}$$

Refer to Table 4 for the moment expressions in the central region and end region.

**Table 4.** Moment expressions.

Load Type	Max. M	M	Domain
Two equal concentrated loads, symmetrical ( $k = a/L$ )	$Pa$	$Pa$	$a \leq x \leq L - a$
		$Px$	$0 \leq x \leq a$

Based on the FEA [6] of an example problem (loads at third points; both 12 and 48 element models), as well as the closed-form solution, the maximum bending stress in the central region did not occur at the midspan but rather near a concentrated load. The difference was a few percent (2.7%). An effective section modulus ( $S_e$ ) can be calculated by evaluating the ratio of maximum moment ( $M$ ) to the maximum stress, which is either  $f_{11}$  or  $f_{22}$  (see prior equations).

Shear flow ( $q_c$ ) can be calculated for the central and end regions by first determining  $V_c$  using the pertinent integration constants for each region. Note that in the central region, for this new load type, the overall shear is essentially zero and the total moment is constant. However, based on an example beam (loads at third points; 48 elements), the core shear and shear flow are not zero in most of the central region, especially near the concentrated loads. The uniform moment is being resisted by the faces' individual flexural stiffnesses, as well as the coupling of faces' axial forces via the core's shear stiffness. The maximum core shear and shear flow occur at the supports.

### 3. Overhang Study Using FEA

This section presents an analytical (FEA) study of composite thermal-barrier beams with unloaded symmetrical overhangs and a midspan concentrated load (Figure 3). No comparisons with experimental data are included. The focus was on the stiffening effect of various overhang lengths on the midspan deflection of this type of sandwich beam. One span ( $L = 1219$  mm (48 in)), with overhangs of length  $a_o$  where  $0 \leq a_o \leq 2L$ , was studied. Two values (138 MPa and 552 MPa) (20 ksi and 80 ksi) of the installed core's effective shear modulus ( $G_{ce}$ ) were used. Two profiles were included: an unsymmetrical (K-1; Figure 4a) and a nominally symmetrical (F-1; Figure 4b) cross-section. Both are based on AAMA (now FGIA) test shapes [2], which are approximately 84 mm (3.31 in) deep and have a polyurethane core (thermal barrier) between the aluminum facing sections.

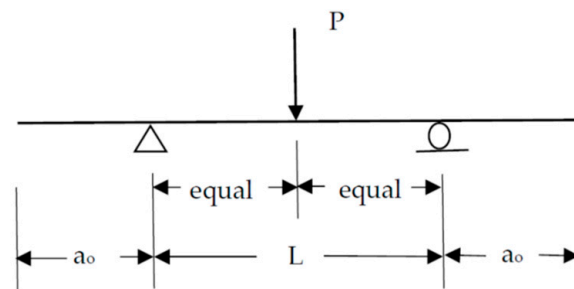


**Figure 3.** Beam with midspan load and overhangs.

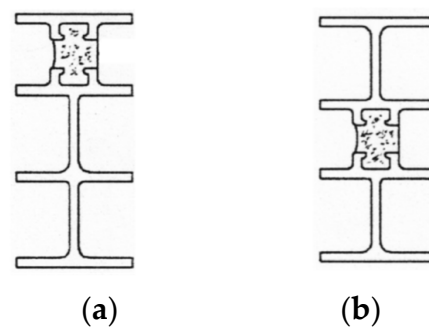


**Figure 4.** Profiles: (a) K-1 (unsymmetric); (b) F-1 (symmetric).

It was learned in research in the 1980s [1] that unloaded overhangs can increase the stiffness of the main span of this type of beam, as compared to a simple span beam with no overhangs. This is due to the shear flexibility of the core, which is much greater than that of the aluminum faces. The AAMA TIR-A8 ([2] (p. 46)) suggests limiting the overhangs on test beams to half of the depth. This is so that the conditions more closely conform to the ideal conditions used for the TIR's predictive equations for simply supported beams without overhangs. Some minimal overhang is needed for practical reasons to provide adequate bearing at the supports. After the research in the 1980s and the initial edition (dated 1990) of the TIR-A8, the software TB-FEM [6] was developed in the 1990s that utilizes a special finite element to incorporate major characteristics of this type of sandwich beam. This software was used for the present analytical study.

Beam tests (midspan deflection in response to midspan concentrated load) are often used in the U.S. to determine the effective shear modulus ( $G_{ce}$ ) of an installed thermal barrier material. Thus, to improve the accuracy of these values, it is desirable to determine the potential size of the stiffening effect of unloaded overhangs on the central span.

### 3.1. Analyses

For each point in the plots (Figures 5 and 6), TB-FEM was used to calculate the midspan deflection. A great amount of other numerical information (e.g., moments, stresses, shear flow, etc.) was also generated but is not part of this discussion. For the profile K-1 and  $G_{ce} = 138$  MPa (20 ksi), coarse models (610 mm (24 in) elements) with 2438 mm, 1219 mm and 610 mm (96 in, 48 in and 24 in) overhangs were used, as well as corresponding finer models (152 mm (6 in) elements). The respective midspan deflections were identical, based on the available four significant figures. Overhangs of 457 mm (18 in) and less had at least three elements. Deflections for coarse and fine meshes were also the same for the beam with no overhangs. For the case of no overhangs, the TB-FEM midspan deflections for all four combinations of the profile and  $G_{ce}$  equaled those based on the corresponding closed-form equations in [2] (pp. 43–61).

For results of the study, refer to the plot in Figure 5 for the unsymmetrical shape and Figure 6 for the symmetrical shape. The stiffening effect is shown as the ratio of the maximum midspan deflection with overhangs ( $y_{cs}$ ) to the base value of deflection with no overhangs ( $y_{BS}$ ). The TB-FEM deflection due to bending was added to the relatively small deflection (0.10 mm (0.004 in)) due to the faces' shear, in order to obtain the total deflections ( $y_{cs}$  and  $y_{BS}$ ). For convenience, the load ( $P$ ) was set at 1779 N (400 lbs) for which total deflections ranged from 2.03 mm to 3.18 mm (0.080 in to 0.125 in). Although not shown in these plots, the stiffening effect for both values of  $G_{ce}$  was the same at  $a_o = 2L$  as it was at  $0.5L$  and  $1.0L$ . Note that, as calculated in prior studies of these beams with no overhangs, the beam stiffness with a given overhang length is not directly proportional to  $G_{ce}$ .

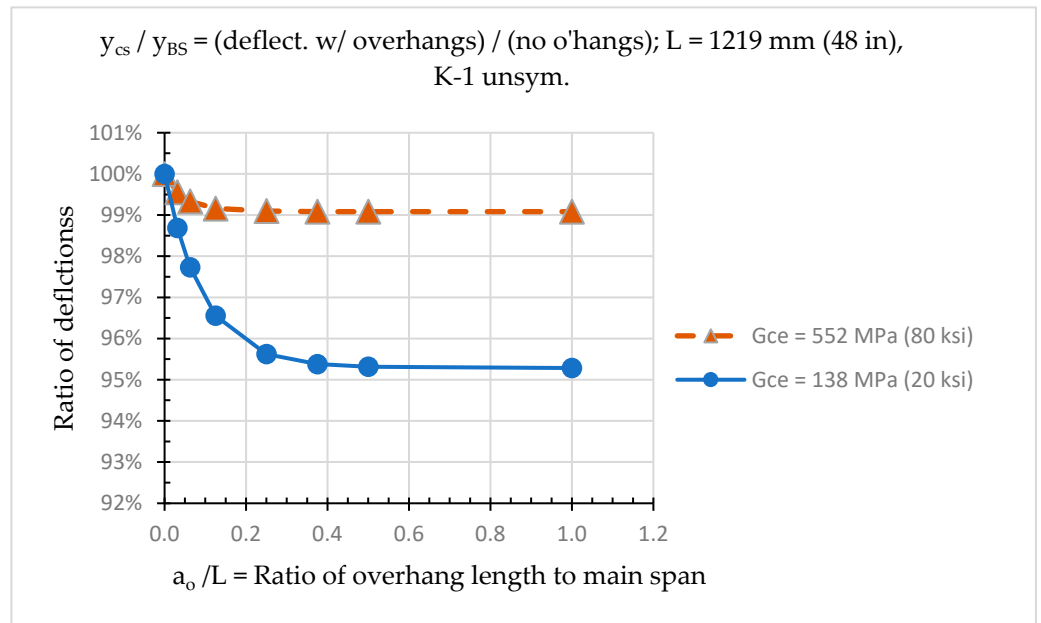


Figure 5. Deflection ratios for profile K-1 (not symmetric).

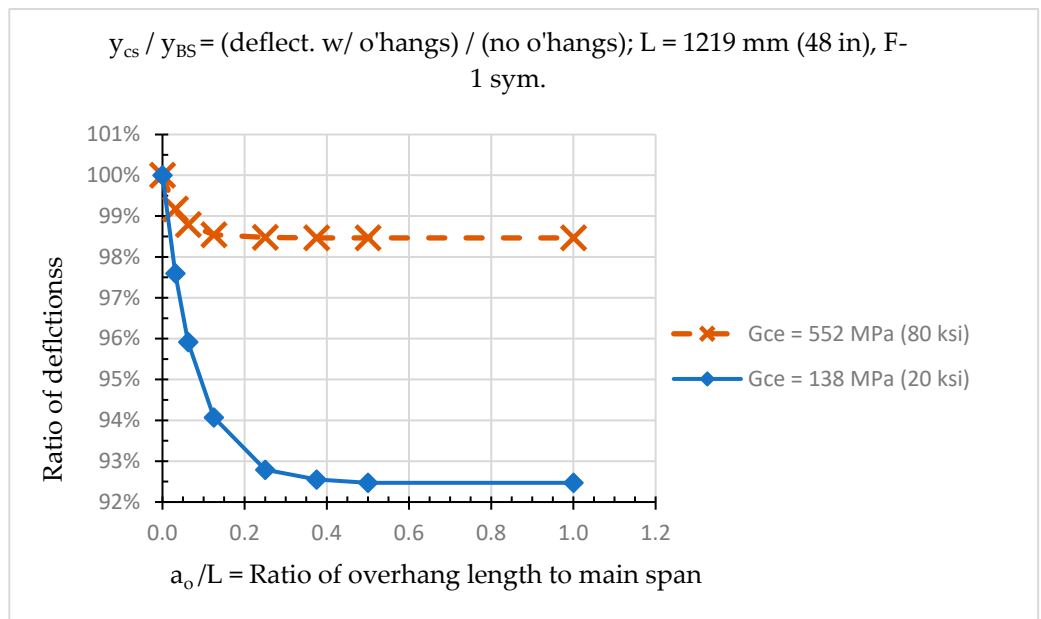


Figure 6. Deflection ratios for profile F-1 (symmetric).

In both figures, for  $G_{ce} = 138 \text{ MPa (20 ksi)}$ , the percentage effect of stiffening (related to the reduction in the midspan deflection) is greatest for overhang lengths of at least  $0.5L$ . In contrast, for  $G_{ce} = 552 \text{ MPa (80 ksi)}$  in both figures, the largest stiffening effect applies for  $a_o \geq 0.25L$ .

The percentage stiffening effect is larger for  $G_{ce} = 138 \text{ MPa (20 ksi)}$ . For the unsymmetric profile (Figure 5), the deflection decrease is about 5% maximum (more precisely 4.7%) for sufficiently long overhangs. For the symmetric profile (Figure 6), the decrease in deflection is about 8% maximum (more precisely 7.5%) for sufficiently long overhangs. For the same load and span, the symmetric profile has a higher shear flow (force per unit length)—and hence a larger longitudinal shear deformation—than the unsymmetric profile. Therefore, for  $G_{ce} = 138 \text{ MPa (20 ksi)}$ , the symmetric shape gained a greater percentage benefit from a given overhang’s stiffening effect.

For  $G_{ce} = 552$  MPa (80 ksi), the stiffening is significantly less pronounced. In Figure 5, the deflection reduction is a maximum of 0.9%, and in Figure 6 it is 1.5%.

The shortest overhang studied was  $a_o = L/32 = 38.1$  mm (1.5 in). This is close to half of the profile's depth (approximately 41.9 mm (1.65 in)). For  $G_{ce} = 138$  MPa (20 ksi), the reduction in deflection varied from 1.3% for the unsymmetric shape to about 2.4% for the symmetric shape. For  $G_{ce} = 552$  MPa (80 ksi), the corresponding reductions are less than 1%.

### 3.2. Comments

If a test beam's midspan deflection experiences a significant effect (reduction) from overhang stiffening, the  $G_{ce}$  value would be overestimated if the TIR-A8 [2] equations for a no-overhang condition were used. For example, if the true  $G_{ce} = 138$  MPa (20 ksi) for the no-overhang case, then a test beam with overhangs of  $a_o = 0.5L = 610$  mm (24 in) would make it appear that  $G_{ce}$  was larger than it really was. Based on a spreadsheet for the unsymmetric profile K-1 with many values of  $G_{ce}$  (increments of 14 MPa (2 ksi)) and corresponding beam stiffnesses for a 1219 mm (48 in) span, a 5% increase in beam stiffness from that (742.2 N/mm (4238 lbs/in)) at 138 MPa (20 ksi) results in a beam stiffness of 779.3 N/mm (4450 lbs/in). This stiffness increase is rounded for illustration. This stiffness in turn corresponds to  $G_{ce} \approx 194.4$  MPa (28.2 ksi), based on interpolation. This is a 41% overestimate of  $G_{ce}$ .

For the symmetric shape (F-1), an 8% increase (rounded for this example) in beam stiffness from 561.1 N/mm (3204 lbs/in) at 138 MPa (20 ksi) produces a stiffness of 605.9 N/mm (3460 lbs/in). This corresponds to  $G_{ce} \approx 181.3$  MPa (26.3 ksi), which is a 31% overestimate of  $G_{ce}$ .

## 4. Conclusions

Part 1 introduced the topic of aluminum beams with composite thermal barriers. In addition, a closed-form solution for the case of two equal concentrated loads (symmetrically located) on a simply supported sandwich beam with no overhangs has been presented. This solution, for deflection, stress and longitudinal shear flow, may be used to analyze this type of "soft core" (thermal barrier) beam, which has a constant moment between the concentrated loads.

Also, the potentially significant effect of unloaded overhangs on the midspan deflection due to a midspan concentrated load of the composite thermal-barrier beams has been considered. For the limited cases studied analytically (one span, two profiles and two values of the core's effective shear modulus ( $G_{ce}$ )), the maximum reduction in deflection was approximately 5% for the unsymmetric profile and 8% for the symmetric profile. Both maximums occurred with the lower  $G_{ce}$  of 138 MPa (20 ksi). As expected, within a certain overhang length range (starting at zero), the stiffening effect increases with the overhang length. However, beyond a certain overhang length ( $0.5L$  for  $G_{ce} = 138$  MPa (20 ksi), and  $0.25L$  for  $G_{ce} = 552$  MPa (80 ksi)), the stiffening effect remains constant.

**Funding:** This research received no external funding.

**Institutional Review Board Statement:** Not applicable.

**Informed Consent Statement:** Not applicable.

**Data Availability Statement:** No physical testing was conducted and hence no new data are available.

**Conflicts of Interest:** The author declares no conflict of interest.

## Abbreviations

### Notation

$A$	shear area of aluminum “web”;
$A_c$	cross-sectional area of core;
$a_1, a_2$	area of Face 1 and 2, respectively;
$b$	$=A_c/D_c$ = average core width;
$c$	$=G_p/(EI_o)$ ;
$c_{11}, c_{22}$	distance between face centroid and air-side surface of Faces 1 and 2, respectively;
$D$	distance between centroids of facing sections;
$D_c$	core depth (maximum);
$E$	Young’s modulus of aluminum faces;
$G_{ce}$	effective shear modulus of installed core material;
$G_p$	$=IbD^2G_{ce}/(I_cD_c)$ ;
$I$	moment of inertia of composite cross-section (no core or face shear effects) $= I_o + I_c$ ;
$I_c$	$=a_1a_2D^2/(a_1 + a_2)$ ;
$I_e$	effective moment of inertia, including core shear effects;
$I'_e$	effective moment of inertia, including core and faces’ shear effects;
$I_o$	$=I_{o1} + I_{o2}$ ;
$I_{o1}, I_{o2}$	moments of inertia of Faces 1 and 2, respectively;
$L$	span length;
$M$	bending moment at distance $x$ from left support;
$V$	shear at distance $x$ from left support;
$x$	coordinate, starting at the left end of the beam.

## References

1. LaBelle, J. Structural Behavior of Aluminum/Elastomer Sandwich Beams. Ph.D. Thesis, University of Wisconsin-Milwaukee, Milwaukee, WI, USA, 1990.
2. LaBelle, J.; Davies, M. Structural Design Method for Composite Aluminum/Elastomer Beams. In *Structural Performance of Composite Thermal Barrier Framing Systems*; AAMA TIR-A8-16; American Architectural Manufacturers Association (AAMA, now FGIA): Schaumburg, IL, USA, 2016; pp. 33–61.
3. Hartsock, J.A.; Chong, K.P. Analysis of Sandwich Panels with Formed Faces. *J. Struct. Div.* **1976**, *102*, 803–819. [[CrossRef](#)]
4. Huang, S. Investigation of Composite Façade Mullions. Ph.D. Thesis, University of Technology Sydney, Sydney, Australia, 2014. Available online: <https://opus.lib.uts.edu.au/handle/10453/29258> (accessed on 21 April 2023).
5. Davies, M. (Scotland, UK). Personal communication, 2000.
6. Wolf, K. *TB-FEM*. Engineering Software Utilizing a Special-Purpose Finite Element for Sandwich Beams (with User’s Guide). 1996, *Unpublished work*.

**Disclaimer/Publisher’s Note:** The statements, opinions and data contained in all publications are solely those of the individual author(s) and contributor(s) and not of MDPI and/or the editor(s). MDPI and/or the editor(s) disclaim responsibility for any injury to people or property resulting from any ideas, methods, instructions or products referred to in the content.